

# Orbital ordering and enhanced magnetic frustration of strained BiMnO<sub>3</sub> thin films

C.-H. YANG<sup>1</sup>, T. Y. KOO<sup>2</sup>, S.-H. LEE<sup>1</sup>, C. SONG<sup>1</sup>, K.-B. LEE<sup>1</sup> and Y. H. JEONG<sup>1</sup>

<sup>1</sup> *Department of Physics & Electron Spin Science Center and* <sup>2</sup> *Pohang Accelerator Laboratory, Pohang University of Science and Technology, Pohang, 790-784, S. Korea*

PACS. 75.50.Dd – Nonmetallic ferromagnetic materials.

PACS. 75.80.+q – Magnetomechanical and magnetoelectric effects, magnetostriction.

PACS. 61.10.Eq – X-ray scattering (including small-angle scattering).

**Abstract.** – Epitaxial thin films of multiferroic perovskite BiMnO<sub>3</sub> were synthesized on SrTiO<sub>3</sub> substrates, and orbital ordering and magnetic properties of the thin films were investigated. The ordering of the Mn<sup>3+</sup>  $e_g$  orbitals at a wave vector ( $\frac{1}{4}\frac{1}{4}\frac{1}{4}$ ) was detected by Mn K-edge resonant x-ray scattering. This peculiar orbital order inherently contains magnetic frustration. While bulk BiMnO<sub>3</sub> is known to exhibit simple ferromagnetism, the frustration enhanced by in-plane compressive strains in the films brings about cluster-glass-like properties.

Orbital degrees of freedom play a critical role in determining the physical properties of transition-metal oxides [1, 2]. BiMnO<sub>3</sub> with manganese electronic configuration of  $t_{2g}^3 e_g^1$  is such an example where  $e_g$  orbital ordering is of central importance. BiMnO<sub>3</sub> is particularly interesting, because it belongs to so-called multiferroic materials which is currently of immense interest [3]. The different degrees of freedom of the system such as electric polarization, orbital, and magnetic spin compete with each other, and ferroelectricity, orbital ordering, and ferromagnetism manifest themselves [4]. This complex multiferroic behavior is already apparent from the chemical formula; Bi<sup>3+</sup> carries a stereochemically active  $6s^2$  lone pair which induces a local distortion and bonding between Bi and neighboring oxygens [5], while Mn<sup>3+</sup> is Jahn-Teller (JT) active and has its share in both the orbital and spin degrees of freedom. Since Mn orbital ordering is necessarily coupled to the distortion caused by the Bi lone pair and also determines the magnetic interaction [6], the detailed knowledge of the orbital ordering would be essential to the understanding of the multiferroic system BiMnO<sub>3</sub>.

Despite recent results regarding BiMnO<sub>3</sub> such as first principle calculations [7, 8], neutron diffraction [9, 10], magnetocapacitance effects [11], and thin film properties [12–14], the orbital ordering pattern and its influences on the ferromagnetic and/or ferroelectric properties await detailed experimental investigations. One factor hindering progress has been the lack of quality samples in bulk or thin film form. However, we have succeeded in obtaining high quality, epitaxial *thin films* and this allowed us to address the issues related to the orbital ordering. In this article, we wish to accomplish two major objectives: first, we will present the resonant x-ray scattering (RXS) data for epitaxial films as a *direct* evidence which confirms the rather peculiar orbital ordering pattern for BiMnO<sub>3</sub> derived previously by Atou et al. from neutron

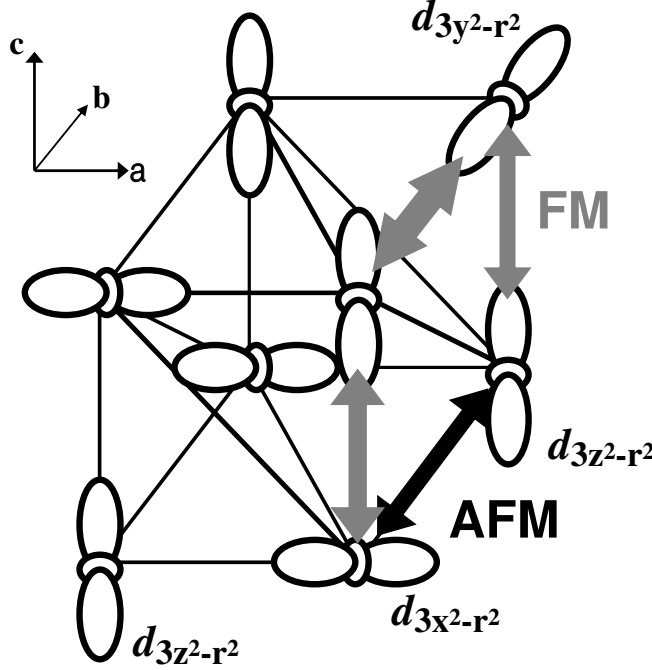


Fig. 1 – The Mn  $e_g$  orbitals in BiMnO<sub>3</sub> are shown; Bi and O ions are omitted. The actual structure of BiMnO<sub>3</sub> is monoclinic with space group  $C2$ . The superexchange interactions indicated by gray and black arrows are ferromagnetic and antiferromagnetic, respectively. Notice that frustration occurs in the plaquette. The thickness of the arrows implies the strength estimated from ref. [17].

diffraction refinements [9]. Second, we wish to demonstrate the magnetic consequences of the orbital order, that is, the *frustration* inherent in BiMnO<sub>3</sub> due to its orbital order manifest itself in the magnetic properties of strained thin films.

From the refinement of the neutron powder diffraction data at room temperature the space group (monoclinic  $C2$ ) and local bond lengths and angles of BiMnO<sub>3</sub> were all determined previously [9, 10]; these structural data contain information on the orientation of JT-distorted MnO<sub>6</sub>'s, from which the compatible ordered pattern of the  $e_g$  orbitals of Mn<sup>3+</sup> ions was inferred by Atou et al.. The orbital order of BiMnO<sub>3</sub>, illustrated schematically in Fig. 1, is rather peculiar in the sense that each plane parallel to (111) contains only one kind of the  $e_g$  orbital within the plane and the stacking sequence goes as  $d_{3z^2-r^2}/d_{3x^2-r^2}/d_{3z^2-r^2}/d_{3y^2-r^2}/d_{3z^2-r^2}/d_{3x^2-r^2}/\dots$ . Thus a superlattice modulation would occur at wavevector  $(\frac{1}{4}\frac{1}{4}\frac{1}{4})$  (in cubic reciprocal lattice unit; the subscript  $m$  is attached to monoclinic indices.). It is noted that the expected orbital order of BiMnO<sub>3</sub> is rather different from that of a similar compound LaMnO<sub>3</sub> at  $(\frac{1}{2}\frac{1}{2}0)$  [15].

According to Goodenough, the superexchange interaction between Mn<sup>3+</sup> ions becomes antiferromagnetic (AFM) when both  $e_g$  orbitals point perpendicular to the bond direction, while the ferromagnetic (FM) interaction prevails when one of the  $e_g$  orbitals points along the bond direction [16]. The striking consequence of the rule in this case is the presence of frustration as indicated in Fig. 1. In bulk BiMnO<sub>3</sub>, however, the FM interactions seem to dominate over the AFM ones and consequently the normal FM ground state results [10]. Since thin films are generally strained and the superexchange interaction depends sensitively on the inter-ion distance, a possibility exists that strains drive the system to a point where

the strength of the FM and AFM interactions are balanced [17]. This then suggests that frustration come into operation and induce a frustrated state in  $\text{BiMnO}_3$  thin films. Thus magnetic properties of thin films are of keen interest.

$\text{BiMnO}_3$  films were grown on  $\text{SrTiO}_3$  substrates from a bulk target via pulsed laser deposition. The substrate temperature was maintained at  $460^\circ\text{C}$  during deposition and the oxygen partial pressure was kept at 4 mTorr [14]. Note that the growth temperature of  $460^\circ\text{C}$  is rather low compared to  $700\sim 750^\circ\text{C}$  adopted by some other groups [12,13]. While these groups used targets with excessive Bi contents to compensate for Bi evaporation during film growth, the low deposition temperature we used presented an advantage of suppressing Bi evaporation and led to a single phase, epitaxial films. X-ray absorption measurements proved that the Mn ions attain the valence of  $3+$  and SEM-EDX indicated that  $\text{Bi:Mn} = 1:1$  within its resolution. The surface roughness measured by atomic force microscopy was  $\sim 5 \text{ \AA}$ . The thickness of the films was estimated from X-ray reflectivity measurements.

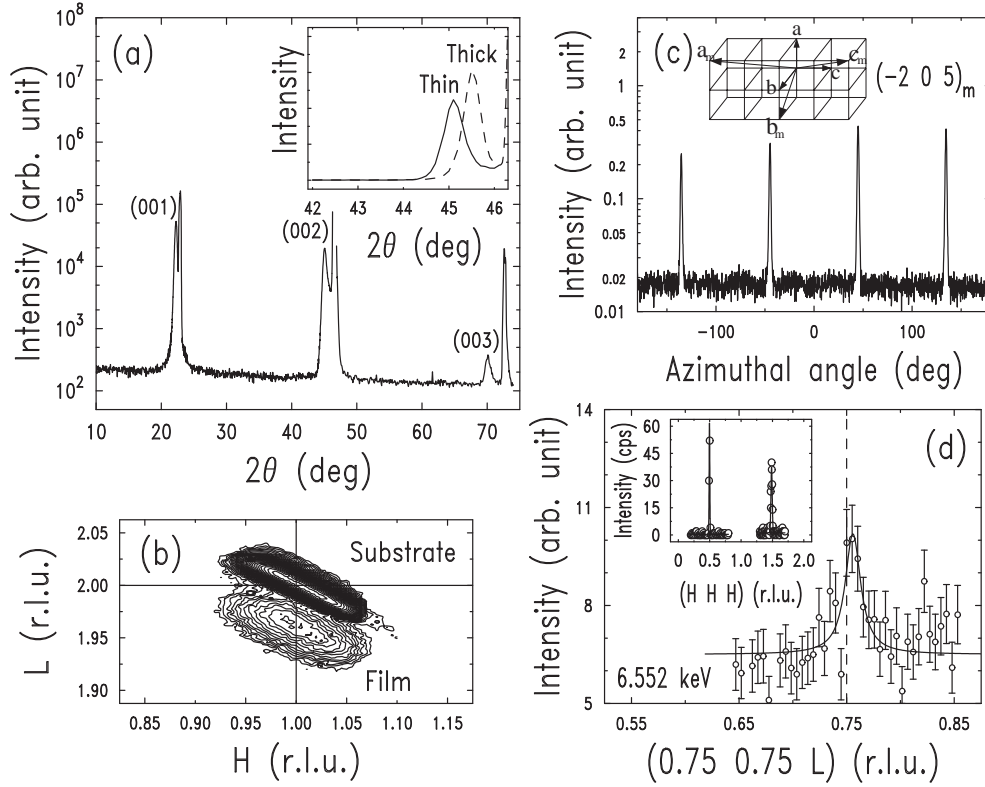


Fig. 2 – X-ray diffraction results for  $\text{BiMnO}_3$  films on  $\text{SrTiO}_3(001)$  substrates. (a)  $\theta - 2\theta$  scan of a film with thickness 40 nm. Inset illustrates the (002) peak for two films of different thickness (solid line, 40 nm; dashed line, 70 nm). (b) Reciprocal space mapping of the 70 nm film around the  $\text{SrTiO}_3$  (102) peak. The tetragonality factor  $t = +1.5 \%$  with  $c$ -axis elongation and in-plane compression. (c) Monoclinic  $(205)_m$  peak which is  $31.2^\circ$  off from the surface normal shows a four-fold symmetry from twinning under azimuthal rotation. Inset describes the relationship between the monoclinic and simple cubic cell. (d) Resonant x-ray scattering peak at Mn K-absorption edge from the 70 nm film. The line is guide to the eye. Inset displays non-resonant superlattice reflections at  $(\frac{1}{2} \frac{1}{2} \frac{1}{2})$  and  $(\frac{3}{2} \frac{3}{2} \frac{3}{2})$ .

Fig. 2 summarizes the x-ray diffraction results at room temperature for two films with thickness approximately 40 nm and 70 nm deposited on  $\text{SrTiO}_3(001)$  substrates. X-ray diffrac-

tion measurements were carried out using synchrotron radiation of the Pohang Light Source (PLS). The  $\theta$ - $2\theta$  scan of the film with thickness 40 nm is presented in Fig. 2(a). The inset illustrates that the 40 nm film has a larger out-of-plane ( $c$ -axis) lattice parameter than that of the film with thickness 70 nm. Fig. 2(b) is the mapping of the (102) peak of the 70 nm film, and shows that the film has an epitaxial relationship with the substrate. The in-plane lattice constant  $a$  is obtained from the Bragg peak position. The films are under in-plane compression and out-of-plane expansion; the tetragonal strain factor, defined as  $t \equiv (c - a)/a$ , is +1.5 % for the thick film (70 nm) and +2.8 % for the thin one (40 nm). The in-plane compression would strengthen the AFM interactions depicted in Fig. 1, and thus enhance frustration.

While tetragonality was adopted to describe the BiMnO<sub>3</sub> films, their exact symmetry is still monoclinic (space group  $C2$ ) with the unique two-fold axis (monoclinic  $b$ -axis) lying in the surface plane. The determination of the symmetry was carried out by searching for several specific monoclinic reflections from the films. A representative Bragg peak  $(\bar{2}05)_m$  of the 70 nm film is displayed in Fig. 2(c); the four peaks appearing as a function of azimuthal angle indicate the existence of naturally occurring 4-fold twins. In the inset of Fig. 2(c) illustrated is the monoclinic unit cell of BiMnO<sub>3</sub>, which is related to the cubic one via the transformation matrix,  $(a \ b \ c)_m = (a \ b \ c)(1 \ -1 \ 1/1 \ 1 \ 1/-2 \ 0 \ 2)$ . The monoclinic lattice parameters were determined as:  $a_m = 9.820 \text{ \AA}$ ,  $b_m = 5.441 \text{ \AA}$ ,  $c_m = 9.852 \text{ \AA}$ ,  $\beta = 110.0^\circ$  for the 40 nm film, and  $a_m = 9.774 \text{ \AA}$ ,  $b_m = 5.440 \text{ \AA}$ ,  $c_m = 9.790 \text{ \AA}$ ,  $\beta = 109.1^\circ$  for the 70 nm one. The monoclinic structure also produces superlattice reflections at  $(\frac{1}{2} \frac{1}{2} \frac{1}{2})$  and  $(\frac{3}{2} \frac{3}{2} \frac{3}{2})$  (corresponding to monoclinic  $(002)_m$  and  $(006)_m$ , respectively) as shown in the inset of Fig. 2(d).

With the monoclinicity of the films established, let us focus our attention on superlattice peaks from orbital ordering. In this regard, it is worth noting that normal charge scattering due to the  $(\frac{1}{4} \frac{1}{4} \frac{1}{4})$  modulation (or equivalently  $(001)_m$ ) is not completely forbidden, but strongly suppressed in the monoclinic structure. However, the suppression was large enough to allow RXS due to orbital ordering to be observed. Procedures for RXS measurements at PLS were described previously [15]; the measurements were carried out at the Mn K-absorption edge of photon energy 6.552 keV at room temperature. Fig. 2(d) depicts RXS results for the 70 nm film, and a peak due to the  $(\frac{1}{4} \frac{1}{4} \frac{1}{4})$  modulation is clearly seen. Although the peak occurs at the expected position, this fact alone is not sufficient to conclude that it is indeed due to orbital ordering; in addition, azimuthal variation of the RXS intensity with respect to the scattering vector and the polarization dependence need to be checked.

Since the  $[111]$ -direction of the film grown on a SrTiO<sub>3</sub>(001) substrate was not parallel to the surface normal, azimuthal scans turned out to be difficult to perform. Thus for further RXS measurements a new sample of approximate thickness 40 nm was grown on SrTiO<sub>3</sub>(111). The RXS results for the new sample are shown in Fig. 3. Fig. 3(a) shows that the expected superlattice peaks are located at the correct positions as satellites of the (111) main peak. The main peak in the figure was obtained from normal scattering, while the side ones are from resonant scattering. Fig. 3(b) illustrates the resonant nature of the latter peaks. The integrated intensity of the  $(\frac{3}{4} \frac{3}{4} \frac{3}{4})$  peak rises sharply to a maximum at 6.552 keV with a width of about 8 eV, and an increase of fluorescence indicates the Mn K-absorption edge. Note that normal charge scattering persists at off-resonance energies. Since only RXS allows  $\sigma$  to  $\pi$  scattering (here  $\sigma$  and  $\pi$  indicate the polarization perpendicular and parallel to the scattering plane, respectively), we carried out azimuthal scans with the  $\sigma$  to  $\pi$  channel allowed with a polarizer at the detector side. Fig. 3(c) displays the azimuthal angle dependence of the  $\sigma$  to  $\pi$  intensity of the  $(\frac{3}{4} \frac{3}{4} \frac{3}{4})$  peak normalized to that of the (111) fundamental peak; a conspicuous intensity oscillation is seen. The azimuthal angle dependence is the hallmark of RXS from orbital ordering and the thorough analysis including twin effects, the details of which are presented elsewhere [18], yielded the solid line in the figure.

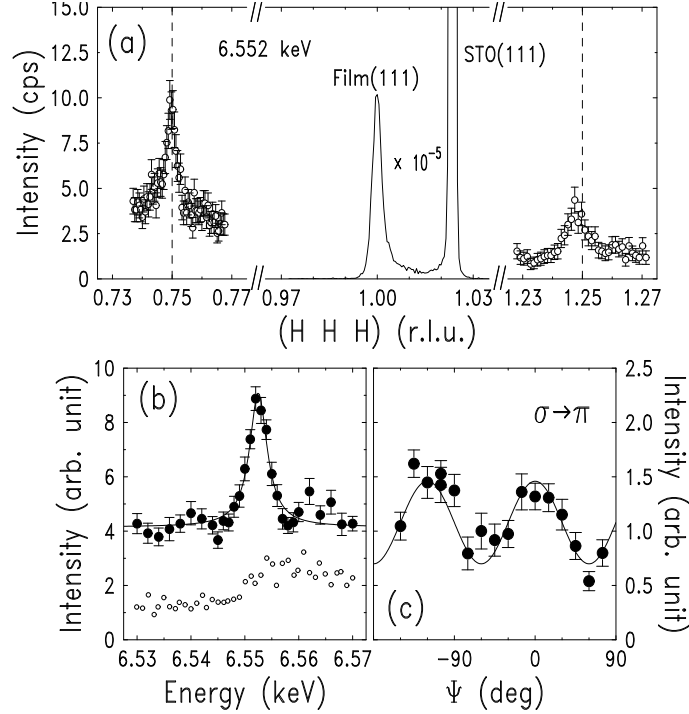


Fig. 3 – Resonant X-ray scattering results for the BiMnO<sub>3</sub> film of thickness 40 nm on a SrTiO<sub>3</sub> (111) substrate. (a) Reciprocal lattice scans along the (111)-direction. The (111) peaks are normal ones, while the peaks at  $(\frac{3}{4}, \frac{3}{4}, \frac{3}{4})$  and  $(\frac{5}{4}, \frac{5}{4}, \frac{5}{4})$  are resonant ones. Notice the intensity difference. (b) The integrated intensity of the  $(\frac{3}{4}, \frac{3}{4}, \frac{3}{4})$  peak as a function of photon energy. The line is a fit to the Lorentzian shape. Also plotted is the fluorescence data (open circles). (c) Azimuthal angle ( $\Psi$ ) dependence of the integrated intensity of the  $(\frac{3}{4}, \frac{3}{4}, \frac{3}{4})$  peak. The intensity is due to scattering from  $\sigma$ -to  $\pi$ -polarization.  $\Psi = 0$  is set when the scattering plane coincides with the  $(1\bar{1}0)$  plane. The line is a sine function with three-fold symmetry.

We now turn to the second major point, that is, the magnetic properties of the BiMnO<sub>3</sub> films; magnetic properties were measured employing a Quantum Design MPMS. In Fig. 4(a), the magnetization  $M$  for the two strained films on SrTiO<sub>3</sub>(001) substrates ( $t = +1.5, +2.8$  % for the 70 and 40 nm thick films, respectively) is plotted as a function of temperature  $T$ . When  $M$  is measured with an in-plane field of 1 kOe (FC, field-cooled),  $M$  increases below a certain temperature, which depends on strain (or thickness) of the film and is much lower than the bulk transition temperature 105 K, as  $T$  is reduced. In addition, the thin films possess smaller saturation moments, when measured under 4 T at 5 K, of  $2.47 \mu_B/\text{Mn}$  ( $t = +1.5$  % film) and  $2.12 \mu_B/\text{Mn}$  ( $t = +2.8$  % film) compared to the bulk value of  $3.6 \mu_B/\text{Mn}$  [10]. More striking is the fact that  $M$  measured with the same field value but first cooled under zero field (ZFC, zero field-cooled) shows deviation from the FC values at low temperatures. The inset of Fig. 4(a) shows that the saturated magnetization of both 40 and 70 nm films, measured at 10 kOe, decreases with temperature displaying the  $T^2$  behavior instead of the well-known  $T^{3/2}$  law [19]. Fig. 4(b) is the plot of  $M - H$  curves for the 70 nm film at selected temperatures. In obtaining these data, magnetic field was applied parallel to the [100] or [010] direction. These measurements were performed after zero-field cooling from 150 K, at which

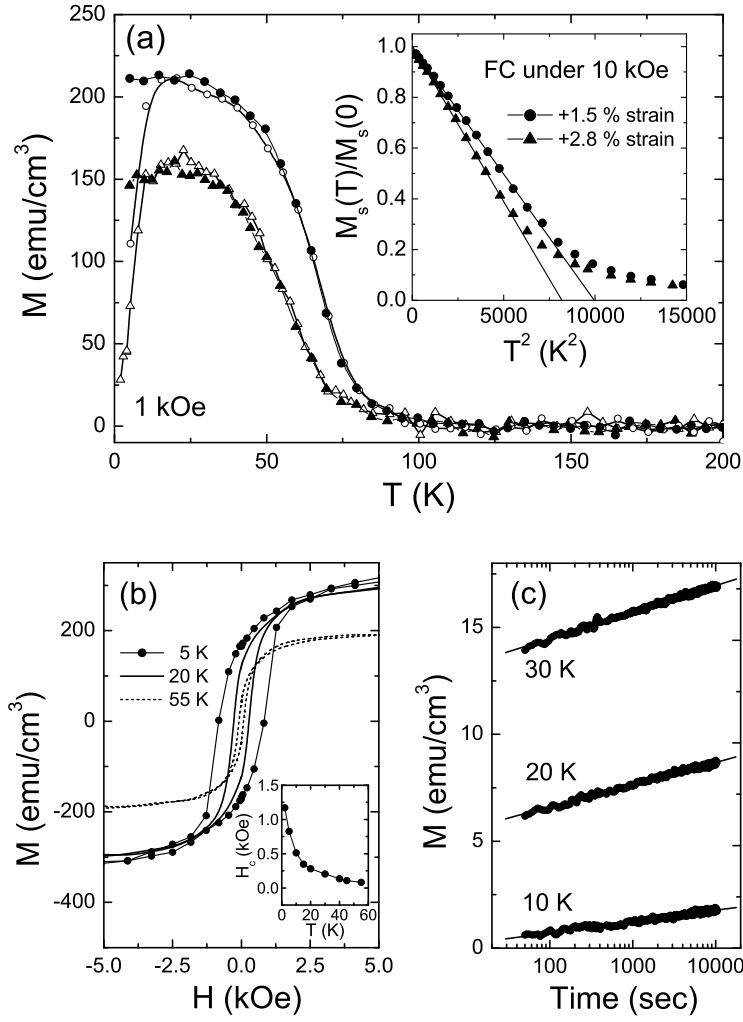


Fig. 4 – Magnetic properties of BiMnO<sub>3</sub> films on SrTiO<sub>3</sub>(001). (a) ZFC (open symbol) and FC (solid symbol) magnetization of the strained films ( $t = +1.5\%$  and  $+2.8\%$ ) is shown as a function of temperature. The in-plane field strength was 1 kOe. Inset displays that the saturation magnetization decreases with the  $T^2$  behavior. (b)  $M - H$  hysteresis curves of the film with  $t = +1.5\%$  at selected temperatures. Inset shows the  $T$  dependence of the coercive field  $H_c$ . (c)  $M$  of the film with  $t = +2.8\%$  is plotted as a function of time. It was zero-field cooled and then a field of 100 Oe was applied. Notice the slow dynamics (time in log scale) with slope increasing with  $T$ .

the film was paramagnetic and didn't show any thermal and field hysteretic behavior. Notice that the coercive field ( $H_c$ ) rapidly increases below the blocking (or freezing) temperature ( $T_b \sim 15$  K).  $T_b$  also indicates the splitting point of ZFC and FC magnetizations in Fig. 4(a).

The magnetic features of the BiMnO<sub>3</sub> films displayed in Fig. 4(a) and (b), a clear difference in FC and ZFC  $M$  values and a rapid increase of  $H_c$  below  $T_b$ , are undoubtedly not those of a typical ferromagnet but of a random magnetic system. Thus to further clarify the magnetic state we sought for time dependent behaviors in  $M$  usually appearing in random systems.

After ZFC a magnetic field of 100 Oe was applied and  $M$  was measured as a function of time. Fig. 4(c) illustrates that  $M$  of the BiMnO<sub>3</sub> film shows a logarithmic behavior in time, and that this relaxational dynamics gets faster with increasing  $T$ . Similar features are often seen in disordered oxide materials and termed 'cluster-glass-like' [20,21]. It is rather remarkable that these unusual magnetic properties are found in BiMnO<sub>3</sub> films without disorder. In this regard it may be worth noting that epitaxial magnetite thin films were also found to possess frustration leading to a magnetic state different from the bulk one [22].

While the detailed account of the magnetic properties of BiMnO<sub>3</sub> films certainly requires further efforts, it may still be concluded that the inherent frustration of BiMnO<sub>3</sub> is enhanced in films with positive tetragonal strain ( $t > 0$ ) and this enhanced frustration alters the FM ground state seen in bulks. Borrowing the theory of superparamagnetism, one may estimate the magnetic cluster size from the measured  $T_b$  and  $H_c$  at zero temperature [23]. The characteristic size estimated in this way is about 3 or 4 nm, and this is sufficiently smaller than the correlation length of the orbital order  $\sim 30$  nm. The latter length is extracted from the width of the x-ray superlattice peak using the Scherrer formula. The clear separation of the two length scales indicates that the anomalous magnetic behavior of the BiMnO<sub>3</sub> films is an intrinsic phenomenon, rather than extrinsic one induced by, for example, finite size domains. In conclusion we thank the financial supports from the SRC program of MOST/KOSEF.

## REFERENCES

- [1] TOKURA Y. and NAGAOSA N., *Science*, **288** (2000) 462.
- [2] MURAKAMI Y. *et al.*, *Phys. Rev. Lett.*, **81** (1998) 582.
- [3] FIEBIG M., *J. Phys. D*, **38** (2005) R123.
- [4] TROYANCHUK I. O., *J. Exp. Theor. Phys.*, **78** (1994) 212.
- [5] SESHADRI R. and HILL N. A., *Chem. Mater.*, **13** (2001) 2892.
- [6] KUGEL K. I. and KHOMSKII D. I., *Sov. Phys. Usp.*, **136** (1982) 231.
- [7] HILL N. A. and RABE K. M., *Phys. Rev. B*, **59** (1999) 8759.
- [8] SHISHIDOU T. *et al.*, *Journal of Physics: Condensed Matter*, **16** (2004) S5677.
- [9] ATOU T. *et al.*, *J. Solid State Chem.*, **145** (1999) 639.
- [10] MOREIRA DOS SANTOS A. *et al.*, *Phys. Rev. B*, **66** (2002) 064425.
- [11] KIMURA T. *et al.*, *Phys. Rev. B*, **67** (2003) 180401(R).
- [12] MOREIRA DOS SANTOS A. *et al.*, *Appl. Phys. Lett.*, **84** (2004) 91.
- [13] SHARAN A. *et al.*, *Phys. Rev. B*, **69** (2004) 214109.
- [14] EERENSTEIN W. *et al.*, *Appl. Phys. Lett.*, **87** (2005) 101906.
- [15] SONG J. H. *et al.*, *Phys. Rev. B*, **66** (2002) R020407.
- [16] GOODENOUGH J. B., *Magnetism and the Chemical Bond* (Wiley, New York) 1963.
- [17] MESKINE H. *et al.*, *Phys. Rev. B*, **64** (2001) 094433. Six different asymmetric positions of oxygen exist in monoclinic BiMnO<sub>3</sub>. Two of them connect neighboring Mn ions along the cubic  $c$ -axis and cause FM interaction ( $J_F^c$ ), while the others are arranged in the  $ab$ -plane and give rise to either AFM ( $J_{AF}^{ab}$ ) or FM interaction ( $J_F^{ab}$ ). Using Mn-O-Mn bulk bond lengths and angles obtained from neutron data, Meskine's theory gives  $J_F^c = -7.9 \pm 0.7$  meV,  $J_{AF}^{ab} = 2.85 \pm 0.05$  meV, and  $J_F^{ab} = -12.0 \pm 0.7$  meV for the Hund energy, say,  $J_H = 1$  eV in BiMnO<sub>3</sub>. The  $\pm$  sign represents variations due to two asymmetric positions per each interaction.
- [18] YANG C.-H. *et al.*, *cond-mat/0601506*, (2006) .
- [19] KÖBLER U., *J. Phys.:Condens. Matter*, **14** (2002) 8861.
- [20] FRETIAS R. S. *et al.*, *Phys. Rev. B*, **64** (2001) 144404.
- [21] MYDOSH J. A., *Spin Glasses* (Taylor & Francis, London) 1993.
- [22] VOOGT F. C. *et al.*, *Phys. Rev. B*, **57** (1998) R8107.
- [23] FONSECA F. C. *et al.*, *Phys. Rev. B*, **66** (2002) 104406.